Spatial time domain reflectometry and its application for the measurement of water content distributions along flat ribbon cables in a full-scale levee model

Alexander Scheuermann,[1] Christof Huebner,[2] Stefan Schlaeger,[3] Norman Wagner,[4] Rolf Becker,[5] and Andreas Bieberstein[1]

Received 4 April 2008; revised 14 November 2008; accepted 9 December 2008; published 19 February 2009.

[1] Spatial time domain reflectometry (spatial TDR) is a new measurement method for determining water content profiles along elongated probes (transmission lines). The method is based on the inverse modeling of TDR reflectograms using an optimization algorithm. By means of using flat ribbon cables it is possible to take two independent TDR measurements from both ends of the probe, which are used to improve the spatial information content of the optimization results and to consider effects caused by electrical conductivity. The method has been used for monitoring water content distributions on a full-scale levee model made of well-graded clean sand. Flood simulation tests, irrigation tests, and long-term observations were carried out on the model. The results show that spatial TDR is able to determine water content distributions with an accuracy of the spatial resolution of about ±3 cm compared to pore pressure measurements and an average deviation of ±2 vol % compared to measurements made using another independent TDR measurement system.

Citation: Scheuermann, A., C. Huebner, S. Schlaeger, N. Wagner, R. Becker, and A. Bieberstein (2009), Spatial time domain reflectometry and its application for the measurement of water content distributions along flat ribbon cables in a full-scale levee model, *Water Resour. Res.*, *45*, W00D24, doi:10.1029/2008WR007073.

1. Introduction

[2] Since the late seventies time domain reflectometry (TDR) has been a well-known and accepted measurement method for determining the water content of soils [*Hoekstra and Delaney*, 1974; *Davis and Annan*, 1977; *Topp et al.*, 1982; *Robinson et al.*, 2003; *Evett and Parkin*, 2005]. Field measurements are often the basis for inversely determined hydraulic properties [*Abbaspour et al.*, 2000; *Ferré et al.*, 2002; *Vereecken et al.*, 2007]. TDR has been proven as a useful tool for the collection of site-specific information, especially for intensive soil sampling [*Long et al.*, 2002; *Stenger et al.*, 2007]. Furthermore TDR can be applied for the monitoring of changes in the water content in geotechnical structures like landfills [*Schofield*, 2001] or in slopes [*Li et al.*, 2005]. Furthermore TDR is used for reference measurements of soil moisture in GPR field applications [*Huisman et al.*, 2003; *Lambot et al.*, 2004; *Serbin and Or*, 2003].

[3] Conventional TDR technology is restricted to the point-wise determination of soil moisture, or mean water content, along a TDR probe with a typical length of 10 to 30 cm [*Robinson et al.*, 2003]. However, many applications in hydrology, agriculture and geotechnical engineering require the determination of the temporal evolution of the water content distribution on larger scales for characterizing soil hydraulic processes in earth structures. The monitoring of a sufficient number of soil moisture profiles is costly, laborious and extremely invasive, if multiple conventional TDR probes have to be installed at different depths. Therefore different approaches based on electromagnetic measurement methods have been proposed for determining water content profiles. The simplest way is to use multisectional transmission lines to receive water content profiles in a limited spatial resolution [*Hook et al.*, 1992; *Feng et al.*, 1999]. One of the first approaches for the inverse determination of moisture profiles was introduced by *Laurent* [2000] which is based on the analysis of the impedance profile of a TDR signal. Another possibility is to develop inversion algorithms based on a straightforward calculation of the wave propagation along the transmission line due to an incident voltage step. Here the response of the transmission line can be calculated either in the time domain [*Lundstedt and Stroem*, 1996; *Lundstedt and He*, 1996; *Feng et al.*, 1999; *Oswald*, 2000; *Todoroff and Lan Sun Luk*, 2001; *Lundstedt and Norgren*, 2003; *Rahman and Marklein*, 2005; *Greco*, 2006] or in the frequency domain [*Norgren and He*, 1996; *Heimovaara et al.*, 2004; *Lambot et al.*, 2004; *Leidenberger et al.*, 2006; *Scheuermann and Huebner*, 2009].

[4] A recently developed reconstruction algorithm [*Schlaeger*, 2002, 2005] allows the fast computation of soil moisture profiles along elongated and electrically insulated probes from TDR signals, using either one- or two-ended measurements. The application of this method leads to an appreciable reduction in the number of probes required accompanied by a higher spatial resolution of the resulting moisture profiles. Probes

[1]Institute for Soil Mechanics and Rock Mechanics, Karlsruhe Institute of Technology, Universität Karlsruhe, Karlsruhe, Germany.
[2]Institute for Industrial Data Processing and Communication, University of Applied Sciences, Mannheim, Germany.
[3]Mathematical Solutions and Engineering, Horn-Bad Meinberg, Germany.
[4]Institute of Material Research and Testing, Bauhaus-University Weimar, Weimar, Germany.
[5]IMKO GmbH, Ettlingen, Germany.

0043-1397/09/2008WR007073

made of flat ribbon cables have proven to be suitable for the quantitative determination of moisture profiles and show much less pulse attenuation than noninsulated probes. The maximal length depends on the surrounding material. For low-loss clean sand the typical maximal length is approximately 5 m. For lossy materials like clay soil or concrete the maximum length should be reduced to approximately 3 m. The two-parameter reconstruction used in the algorithm of *Schlaeger* [2005] explicitly takes into account losses by dissipation as one effect of the electrical conductivity.

[5] The technology of soil moisture profile determination, including measurement devices and probes, reconstruction algorithm and calibration procedures, has been introduced as spatial TDR [*Becker*, 2004; *Huebner et al.*, 2005]. So far spatial TDR has been applied using different methods. It has been implemented with open ended three-rod probes in small catchments in Germany to develop a flood warning system [*Becker*, 2004; *Schaedel*, 2006]. Currently spatial TDR is being used with improved three-rod probes to investigate near-surface moisture dynamics in small catchments. In small-scale applications spatial TDR has been used for the laboratory investigation of water content dynamics in unsaturated soils [*Scheuermann*, 2008]. Most frequently spatial TDR with flat ribbon cables has come into use for the observation of water content changes in levee models [*Scheuermann et al.*, 2001, 2005; *Woersching et al.*, 2006] and also recently in real levees for monitoring purposes [*Scheuermann et al.*, 2008].

[6] A full-scale levee model at the Federal Waterways and Research Institute in Karlsruhe was equipped with a spatial TDR system for the observation of water balance processes in general and for the investigation of the influence of the initial water content distributions on the transient seepage through levees in particular [*Scheuermann*, 2005]. The motivation to use spatial TDR was to permit measurements with a reasonable temporal resolution also at the waterside slope of the levee even if the slope is flooded. Flood simulation tests as well as sprinkler irrigation tests and long-term observations were conducted on the levee model. The measured water content distributions showed a distinctive variability due to the hydraulic boundary conditions for both the spatial distribution as well as for the absolute value of the measured water contents. Here the spatial TDR method is demonstrated with flat ribbon cables, as a special form of transmission line, with two-ended measurements. The application of the method will be presented with the help of the experimental investigations on the levee model. Detailed information on the investigations on the levee model is given by *Scheuermann* [2005], *Scheuermann et al.* [2001], and *Scheuermann and Bieberstein* [2006].

2. Spatial TDR Using Flat Ribbon Cables

2.1. Transmission Line Design

[7] In the simplest design of a TDR probe, noninsulated metallic rods are used as transmission lines in the form of either a two- or a three-rod probe. Many conventional applications use this kind of probe for point-wise measurements of the water content. One advantage of the use of noninsulated metallic rods is the possibility of the direct calculation of the permittivity of the material surrounding the waveguide from the wave velocity [*Whalley*, 1993; *Heimovaara and Bouten*, 1990], which can be determined using simple travel time analysis. However, a serious limitation in the use of uncoated rods is the restricted length, which is limited to a maximum of about 1 m for use in soils because of losses caused by the electric conductivity of the moist soil [*Dalton and van Genuchten*, 1986].

Figure 1. Flat ribbon cable consisting of three copper wires with polyethylene insulation.

[8] For longer transmission lines, insulated flexible flat ribbon cables can be used. They show much less pulse attenuation than uncoated metallic rods in the same medium. Several cables with different geometries have been developed and manufactured in the past, from simple concentric insulation to sophisticated multiwire structures with unilateral sensitivity [*Huebner and Brandelik*, 2000a, 2000b]. The flat ribbon cable used in the presented investigations was originally developed for water content measurements in snow [*Huebner and Brandelik*, 2000a] (see Figure 1). The cable consists of three copper ribbons as wires covered with polyethylene insulation. The advantage of flat ribbon cables is the reduction of the influence from the electrical conductivity on the wave propagation. This permits the use of flat ribbon cables with lengths of up to 40 m, if mean water contents are to be measured [*Stacheder et al.*, 2005]. However, the determination of electrical conductivity is more complicated and less accurate compared to noninsulated probes. It is only possible to obtain information about the conductive behavior of the soil from TDR measurements within certain limitations [*Stacheder*, 1996]. Using insulated probes means there is less influence from soil electrical conductivity on the TDR signal. Consequently, the determination of electrical conductivity from the TDR signal is less accurate than in the case of noninsulated probes. Nevertheless, the advantage of lengthening insulated transmission lines outweighs this minor disadvantage.

[9] In order to predict the time domain response of the cable, the electromagnetic transmission line properties have to be measured in laboratory experiments or calculated by numerical methods on the basis of the equivalent circuit for an infinitesimal section of a transmission line (Figure 2). The equivalent parameters of the circuit are the series resistance R, inductance L, shunt conductance G and capacitance C. The fact that radiation and higher-order modes of electromagnetic wave propagation are not included presents a limitation with this model [*Lundstedt and Stroem*, 1996]. Open wirelines show electromagnetic radiation when the spacing between the wires is comparable or larger than the wavelength of the

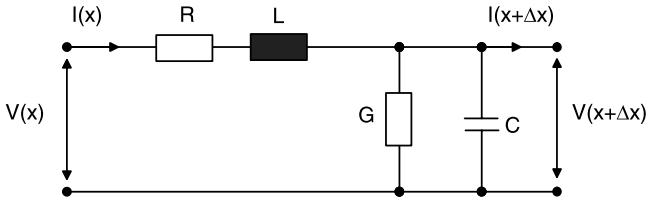

Figure 2. Equivalent circuit of an infinitesimal section of a transverse electromagnetic (TEM) transmission line. $V(x)$ and $I(x)$ are the voltage and the current at the beginning and the end of the line.

electromagnetic signal, thus forming a hybrid transmission line/antenna system. The radiation strongly increases with the frequency and may be a significant source of loss and risetime degradation. However, for common probe designs used in hydrology the equivalent circuit in Figure 2 provides a reasonable approach for calculating the wave propagation along the transmission line. The minimum conditions to be maintained in this case are: wave modes other than the transversal-electromagnetic (TEM) mode and frequency dependence of transmission line properties may be neglected. In the following, the parameters of the equivalent circuit for the flat ribbon cable are presented and discussed on the basis of the equivalent circuit model. The sensitivity of the flat ribbon cable as a transmission line for the measurement of permittivity is discussed in section 2.1.3.

2.1.1. Inductance *L* and Resistance *R*

[10] Both L and R are parameters which are assumed to be constant along the probe. The resistive losses of the flat ribbon cable are influenced by the skin effect. At low frequencies there is a uniform distribution of the current through the cross section of the copper conductors. As the frequency increases, the current is concentrated on the edges of the conductors, and at the highest frequencies most of the current flows in a very thin layer. Consequently, the cross-sectional area available for current flow decreases and causes an increase in series resistance (Figure 3). However, in most practical cases resistance losses are very small compared to dielectric losses (shunt conductance) except with long cables in nearly lossless materials like snow. For this reason, the influence of the resistance R can be neglected when the flat ribbon cable is used in soils [*Huebner et al.*, 2005].

[11] Because of the skin effect the inductance is also dependent on the frequency (Figure 3). Internal inductance

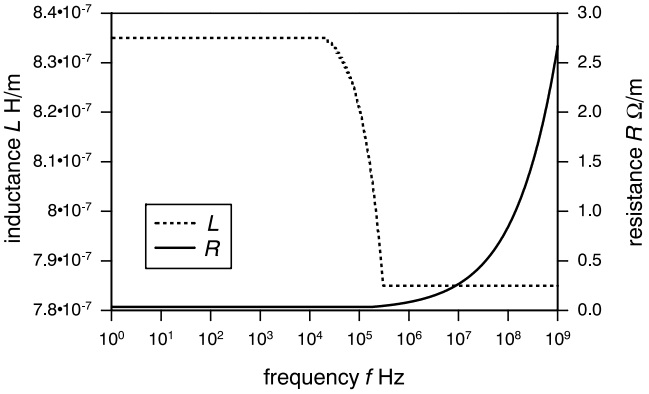

Figure 3. Series resistance and inductance of the flat ribbon cable for symmetric excitation.

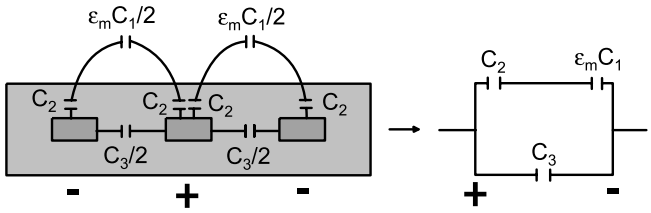

Figure 4. Capacitance model of the flat ribbon cable.

decreases with frequency and only external inductance remains. The transition frequency is around 100 kHz. This means that within the usual time window of TDR measurements (<100 ns, which corresponds to a low-frequency limit of about 10 MHz) no significant influence of the inductance increase at low frequencies is to be expected. The measured external inductance corresponds with that calculated by electromagnetic field calculation [*Huebner*, 1999].

2.1.2. Capacitance *C* and Conductance *G*

[12] Unlike R and L, C and G are dependent on the dielectric properties of the moist soil surrounding the flat ribbon cable. The frequency dependence of the permittivity is considered to be less pronounced in the TDR frequency range. It is possible to derive a relationship between relative permittivity ε_m and C for the flat ribbon cable using a simple capacitance model with the three capacitances C_1, C_2 and C_3 as shown in Figure 4. C_1 considers the influence from the ε_m of the surrounding soil. The other two capacitances take into account the influence of the insulation between conductor and soil (C_2) and between the conductors (C_3). In this way the capacitance model represents a combination of capacitances connected in series and in parallel (Figure 4, right):

$$C(\varepsilon_m) = \frac{\varepsilon_m C_1 \cdot C_2}{\varepsilon_m C_1 + C_2} + C_3 \tag{1}$$

For the lossless case, it is possible to calculate the relation between ε_m and C with full wave numerical field simulation. The capacitance model of equation (1) and the field calculation correspond very well. [*Huebner et al.*, 2005]. Consequently, the capacitance model can be used to parameterize the relationship between ε_m and C. The three unknown capacitances C_1, C_2, and C_3 can be derived either from numerical electromagnetic field calculation or using calibration measurements in the laboratory with three different media around the cable. Normally air ($\varepsilon_{m,a} = 1$) and water ($\varepsilon_{m,b} \approx 80$, depending on temperature) are used as calibration media. As a third medium water saturated glass beads have been proved suitable for calibration purposes, since the resulting permittivity is roughly $\varepsilon_{m,c} \approx 25-30$, which represents approximately the permittivity of saturated soils. The measurements are conducted for probes of a known length. The wave velocity along the transmission line can be calculated using simple travel time analysis. With the known L of the transmission line the mean capacitance along the probe is calculated for the three calibration media with the equation

$$v_i = \frac{1}{\sqrt{L \cdot C_i(\varepsilon_{m,i})}} \tag{2}$$

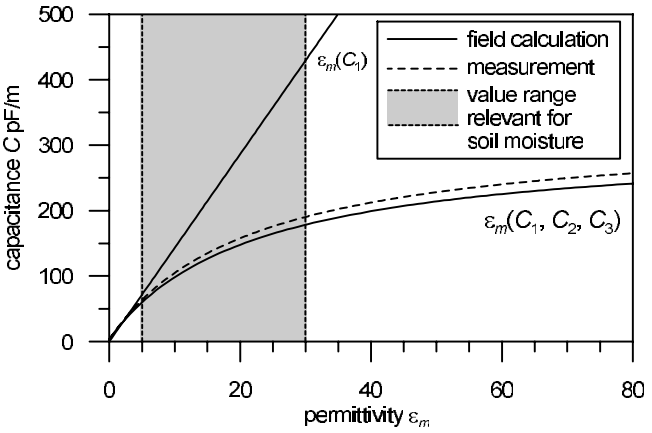

Figure 5. Relation between permittivity and capacitance for the lossless case and symmetric excitation of the cable (Figure 1).

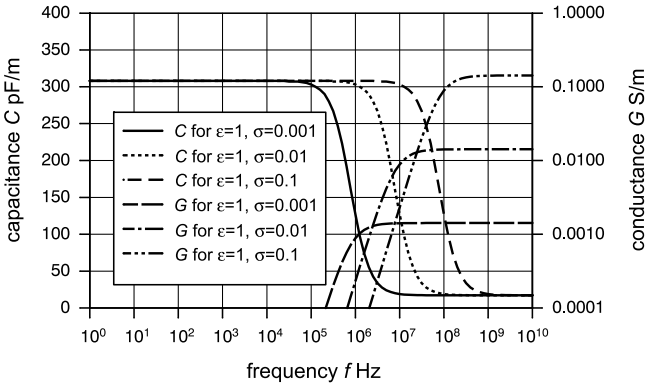

Figure 6. Capacitance C and conductance G of the flat ribbon cable embedded in a material with real permittivity $\varepsilon_m = 1$ and conductivities of $\sigma_m = 0.1$, 0.01, and 0.001 S/m.

for $i = a$, b and c. On the basis of equation (1) and the three capacitances (C_a, C_b and C_c) for the known calibration media the parameters (C_1, C_2 and C_3) can be calculated for the capacitance model. Figure 5 shows a comparison of the relationships between relative permittivity ε_m and C from experimental investigations and electric field calculation. The corresponding parameters are summarized in Table 1. The difference between the measured and numerically calculated parameters can be attributed to uncertainties concerning the thickness of the insulation, which is a very sensitive parameter, especially for high permittivities.

[13] The dielectric losses in the polyethylene insulation are small compared to losses caused by soil conductivity and can therefore be neglected [*Huebner et al.*, 2005]. Only soil remains as a source of electrical losses. It can be shown that the equivalent circuit parameters C and G may have a dispersive behavior, although the electrical properties of the ε_m and conductivity σ_m of the soil are assumed to be frequency independent. This can be attributed to the Maxwell-Wagner effects [*Nyfors and Vainikainen*, 1989]. Figure 6 shows the frequency dependence of C and G of the flat ribbon cable for $\varepsilon_m = 1$ and $\sigma_m = 0.1$, 0.01, and 0.001 S/m. At low conductivities ($\sigma_m < 0.001$ S/m) the dispersion of C and G can be neglected for the dominant frequency range of the TDR signals used for reconstruction ($f > 10$ MHz). The equivalent circuit model is valid for common properties of soils. Only for high conductive conditions (e.g., for saline pore water) does the model need further refinement.

2.1.3. Sensitivity of the Flat Ribbon Cable and Soil Sensor Interaction

[14] The consideration of an idealized equivalent circuit, which is a simplification frequently utilized in TDR applications, does not consider losses due to the skin effect or radiation from the sensor and includes the assumption of a homogeneous sensitivity distribution along the sensor

Table 1. Parameters of the Capacitance Model of the Flat Ribbon Cable

Circuit Element	C_1 (pF/m)	C_2 (pF/m)	C_3 (pF/m)
Measured	14.8	323	3.4
Calculated	13.7	303	4.0

[*Heimovaara et al.*, 2004; *Huebner and Kupfer*, 2007]. On the basis of this model, the sensitivity of a sensor can be defined by two main sensor properties which result from the interaction with the surrounding soil. The first one is related to the sensor specific calibration and corresponds to the changes of the capacitance depending on the soil permittivity. The second property concerns the spatial distribution of the electromagnetic field defining the sensitive area around the sensor.

[15] The sensor specific calibration, defined by the relationship between the real permittivity of the soil ε_m and the measured capacitance C (Figure 5), is the result of the design of the sensor including the geometry and the materials used. In Figure 5 the linear evolution of the relationship between permittivity and capacitance is additionally presented for the hypothetical case of a given design of the flat ribbon cable without insulation. In this case C_2 and C_3 vanish in the capacitance model and C_1 is only dependent on the geometry of the sensor. The differences between measurement and calculation are attributed to the uncertainty in measuring the thickness of the insulation, which is a very sensitive parameter, especially at high permittivities. As can be seen in the graph, the flat ribbon cable shows a satisfactory sensor sensitivity within the range of permittivities related to the water content measurements in soils ($\varepsilon_m = 5$ for dry soils and up to 30 for saturated soils).

[16] The sensitive area around the sensor is strongly dependent on the contact conditions between the sensor and the surrounding material. For this reason the sensitivity of a flat ribbon cable was investigated with 3-D electromagnetic finite element modeling (Ansoft-HFSS, high-frequency structure simulator) taking the frequency-dependent complex dielectric permittivity into consideration [*Wagner et al.*, 2007a]. Figure 7 shows an example of the numerically calculated result of a flat ribbon cable surrounded by air, moist clay and quartz powder as well as natural water. On the top left side of the graph the electric field distribution is given as a 3-D view, and on the top right the cross-sectional distributions for the electric field (above) as well as for the magnetic field (below) are shown. Moreover, longitudinal sections of the cable sensor stimulated with different frequencies are given.

[17] As can be seen in the 2-D and 3-D graphs, the electromagnetic field is concentrated around the conductors

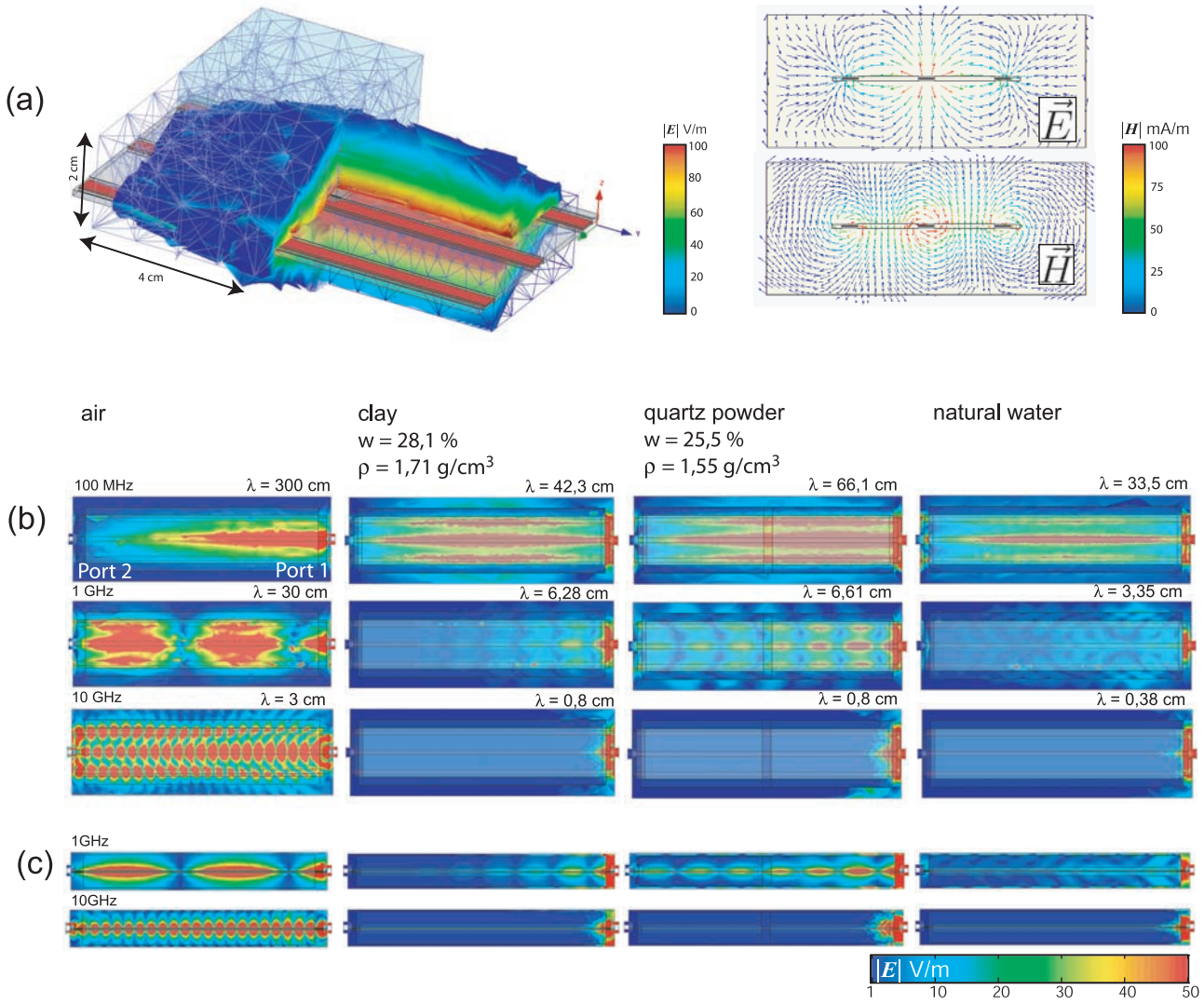

Figure 7. (a) Electric and magnetic field distribution of a flat ribbon cable section surrounded by air at a frequency of 1 GHz. Electric field distribution (steady state standing wave) (b) of a 30 cm flat ribbon cable exited from port 1 with different frequencies surrounded by air, moist clay, quartz powder, and natural water (for details, see *Wagner et al.* [2007a]) for a longitudinal horizontal section and (c) for a longitudinal vertical section of the simulated structure. The appropriate gravimetric water content w, bulk density ρ, and wavelength λ of the surrounding material is indicated.

and defines a sensitive area of 1 cm up to 2 cm on both sides of the sensor cable (Figure 7). However, qualitatively the numerical calculation has shown that the sensitivity characteristic of the flat ribbon cable changes along the sensor depending on the dielectric relaxation behavior of the surrounding material. For highly electrically lossy material, an increase in the TDR risetime as well as a strong absorption of multiple reflections could be observed for increasing volumetric water contents. This finally leads to a frequency-dependent decrease of the spatial resolution and the penetration depth of the electric field (sensitivity region around the sensor) along the flat ribbon cable on the one hand and on the other hand to a limited maximum length of the sensor available for moisture measurements.

[18] One main conclusion of this investigation is that coupling problems caused by air or water gaps lead to dramatic travel time distortion even for very small gaps. An air-filled gap with a thickness of 0.25 mm on both sides of a flat ribbon cable already leads to the drastic underestimation of the water content by approximately 36%. In contrast, a drastic overestimation occurs in the case of a water-filled gap for the same gap size. Therefore, careful installation of the probes and effective probe-soil coupling are essential for the quantitative determination of the in situ water content. The influence of structural changes on the determination of the permittivity was investigated by *Rothe et al.* [1997].

2.2. Spatial TDR Measurement Procedure for Two-Ended Measurements

[19] The setup procedure for two-ended spatial TDR measurements using flat ribbon cables as transmission lines is shown in Figure 8. The differences between this setup and

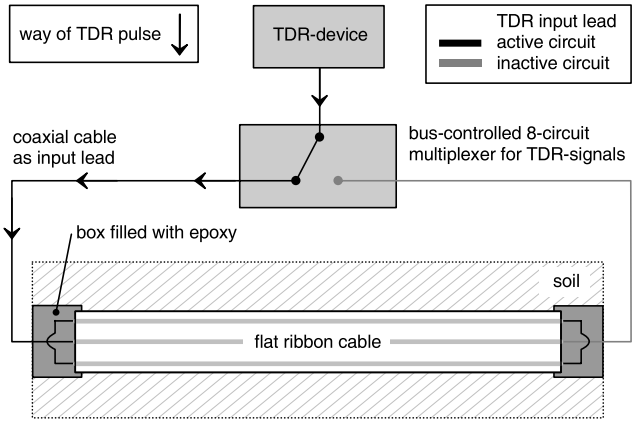

Figure 8. Basic TDR setup and signals. Oscilloscope and pulse generator are usually integrated in a single TDR device.

the setup for conventional TDR measurements mainly concern (1) the electrical boundary conditions at the end of the transmission line and (2) the use of multiplexers for automated measurements. A TDR device, which consists of a pulse generator and an oscilloscope (i.e., Tektronix cable tester 1502B/C or Campbell Scientific TDR100), emits a fast risetime (about 200 ps) voltage step via a bus-controlled multiplexer into a coaxial cable, which acts as an input lead within the active circuit (black line with arrows). The multiplexers are based on a modular design, which also permits large installations at a very low cost. At the transition between the coaxial cable and the flat ribbon cable part of the pulse is reflected because of impedance mismatch. The remaining pulse travels along the flat ribbon cable until it reaches the transition to the second coaxial cable at the opposite end of the flat ribbon cable (Figure 8). At the transition to the flat ribbon cable the inactive circuit (gray line) acts as a 50 Ω boundary condition leading to a further impedance mismatch in the TDR measurement. In highly conductive soils the impedance mismatch may vanish in such a configuration.

[20] The second TDR measurement is conducted from the opposite end of the flat ribbon cable via the second coaxial cable connected with the TDR device via a separate multiplexer channel. The TDR device records the sum of the incident signal and the reflected signal (step response), also called the TDR trace, from which the travel time and the mean wave velocity in the sensor line section can be determined. Although the measurements are conducted from opposite ends of the flat ribbon cable, the mean velocity of both measurements must be equal. This acts as a first indication of the quality of the TDR measurement. An example of an actual two-ended measurement along a flat ribbon cable (without the waveforms along the coaxial cables) is given in Figure 9. As can be seen from the graph, although the information content of both TDR traces is the same, the temporal evolution differs significantly. In particular the time, when the transition from the dry to the wet zone (curve for end 1) or from the wet to the dry zone (curve for end 2) is reached, differs because of the dependence of the velocity on the permittivity of the soil. It is obvious that simple signal analysis cannot provide a spatial analysis of the TDR traces. For this purpose sophisticated inverse strategies are required.

2.3. Soil-Specific Calibration

[21] The relationship between volumetric water content and dielectric permittivity is affected by various factors such as measurement frequency, temperature, mineralogical composition, structure, texture, bulk density and chemical composition of the pore fluid [*Shen et al.*, 1987; *Ishida et al.*, 2000; *Boyarskii et al.*, 2002; *Gutina et al.*, 2003; *Hilhorst et al.*, 2001; *Topp et al.*, 1980; *Logsdon*, 2005]. Therefore, the objective of numerous experimental, numerical and theoretical investigations is the development of general calibration rules for a broad range of soil textures and structures [*Wang and Schmugge*, 1980; *Topp et al.*, 1980; *Roth et al.*, 1990, 1992; *Jacobsen and Schjønning*, 1993; *Friedman*, 1998]. These models are mostly based on the assumption that there is a constant dielectric permittivity in a frequency range around 1 GHz as a function of the volumetric water content [*Sihvola*, 2000; *Behari*, 2005; *Regalado*, 2006].

[22] However, the frequency dependence in the dielectric relaxation behavior below 1 GHz due to a certain amount of clay minerals in soil is not adequately taken into consideration [*Heimovaara et al.*, 2004, *Logsdon*, 2005; *Wagner et al.*, 2007a]. In clay-water systems multiple relaxation processes may occur but these are complicated and poorly understood [*Ishida et al.*, 2003; *Logsdon*, 2005; *Wagner et al.*, 2007a,

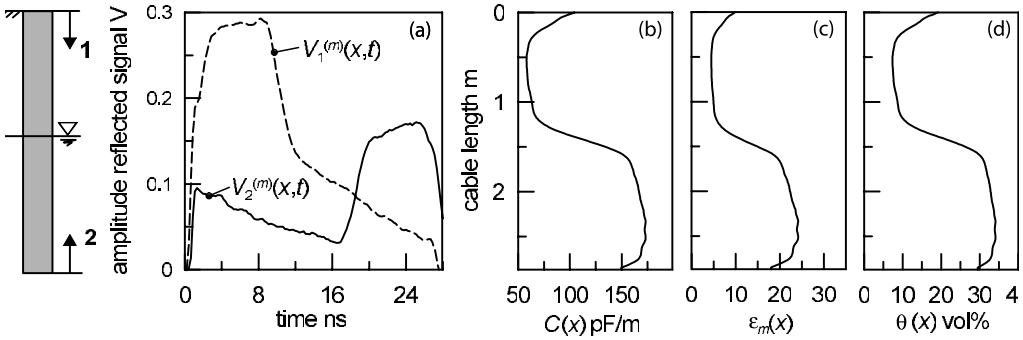

Figure 9. Measurements on a flat ribbon cable (half of the cable is located in saturated soil): (a) reflection data from the top (labeled 1) $V_1^{(m)}(x, t)$ and from the bottom (labeled 2) $V_2^{(m)}(x, t)$ of a flat ribbon cable, (b) spatial distribution of the capacitance, (c) distribution of the real permittivity, and (d) distribution of the volumetric water content. The increase at the top is caused by a vegetated topsoil layer. The decrease below is an artifact of the inverse modeling and is influenced by the steepness of the input signal.

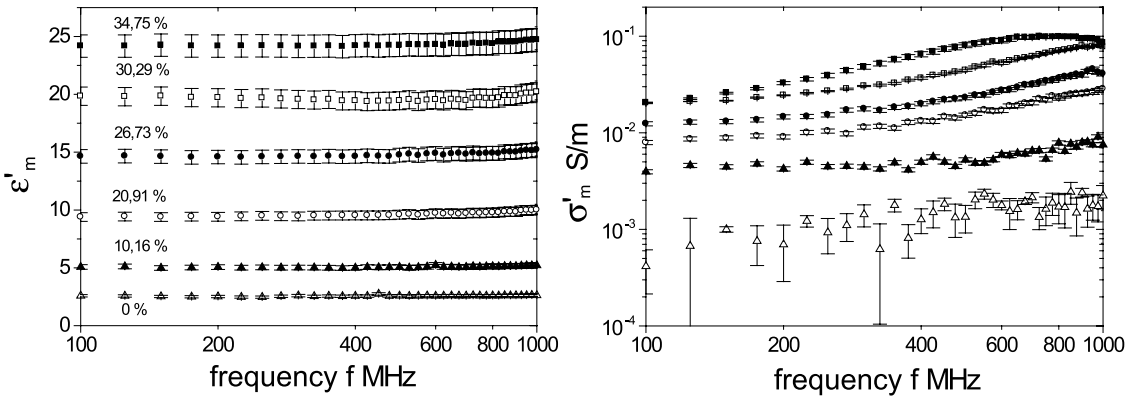

Figure 10. (left) Real part ε'_m of the complex effective relative dielectric permittivity $\tilde{\varepsilon}_m = \varepsilon'_m - j\varepsilon''_m$ and (right) real part σ'_m of the complex effective electrical conductivity $\tilde{\sigma}_m = j\omega\tilde{\varepsilon}_m = \sigma'_m + j\sigma''_m$ as a function of frequency f of the levee model sand for selected volumetric water contents.

2007b, 2007c; *Asano et al.*, 2007]. The levee model soil is a well-graded clay free sand. In order to analyze the frequency dependence, the complex dielectric permittivity of the levee soil was examined in a frequency range from 100 MHz to 1 GHz at room temperature and under atmospheric pressure with a dielectric measurement setup according to *Huebner* [1999]. Selected measurement results are shown as a function of the frequency in Figure 10. As expected, losses and dispersion of the levee soil are very weak. Furthermore, the critical frequency f_C of the soil is expected to be below 1 MHz. Here, f_C defines the boundary between quasi–steady state phenomena and wave phenomena, at which the ratio of the absolute value of conduction current density and displacement current density equals 1 (for details, see *Katsube and Collet* [1974], *Kirsch* [2006], and *Wagner et al.* [2007b]). For these reasons, it is justified to assume that effective dielectric permittivity is constant in the TDR-frequency range and the material calibration with gravimetric sampling is performed at a measurement frequency of 1 GHz. The experimental results of the calibration experiment are given in Figure 11 (black dots).

[23] The complex relative permittivity $\tilde{\varepsilon}_m$ at a frequency of 1 GHz of all the investigated samples was analyzed with a simple three phase mixing model according to *Lichtenecker and Rother* [1931]:

$$\tilde{\varepsilon}_m = \left(\theta \cdot \tilde{\varepsilon}_w^{\alpha} + (1-n)\varepsilon_s^{\alpha} + (n-\theta)\varepsilon_a^{\alpha}\right)^{1/\alpha} \qquad (3)$$

with volumetric water content θ, porosity n, permittivity of air $\varepsilon_s = 1$ of solid mineral grains $\varepsilon_s = 4.5$, the temperature-dependent complex relative dielectric permittivity of free pore water $\tilde{\varepsilon}_w$ according to *Kaatze* [2005] and *Buchner et al.* [1999] and a so-called structure parameter α. In previous broadband investigations of a silty clay loam from a levee along the river Unstrut/Germany it has been shown that structure parameter α and direct current pore water conductivity σ_w depend on the volumetric water content and the porosity [*Wagner et al.*, 2007b, 2007c]. The approach of Wagner et al. is applied to the material from the levee model instead of empirical calibration functions frequently used in soil science (Figure 11). The determination of the volumetric water content from the spatial TDR measurements on the levee model is achieved with this relationship.

2.4. Reconstruction Algorithm

2.4.1. Basic Consideration

[24] The travel time of a reflected electromagnetic signal includes the information of the mean dielectric properties around the probe. However, the full reflectogram contains far more information. The section between the first and second main reflections from the beginning and the end of the probe is a finger print of the dielectric profile along the waveguide, which is dominated by the water content (Figure 9). In order to reconstruct a water content profile from TDR measurements, a procedure has been developed consisting of three steps. This procedure is described in detail by *Schlaeger* [2005]. In the first step the spatially distributed transmission line parameters $C(x)$ and $G(x)$ are reconstructed with two independent measurements from both ends of the flat ribbon cable. If only one TDR measurement is available, we assume $G(x)$ to be constant or related to C(x). This relationship $G(x) = f(C(x))$ has to be determined experimentally and can be used directly in the reconstruction algorithm [*Hakansson*, 1997; *Becker*, 2004]. In the second step $C(x)$ is transformed to $\varepsilon_m(x)$, e.g., for the flat ribbon cable with the help of equation (1). In the third step $\varepsilon_m(x)$ is converted into a water content profile either by standard transformations [*Topp et al.*, 1980] or

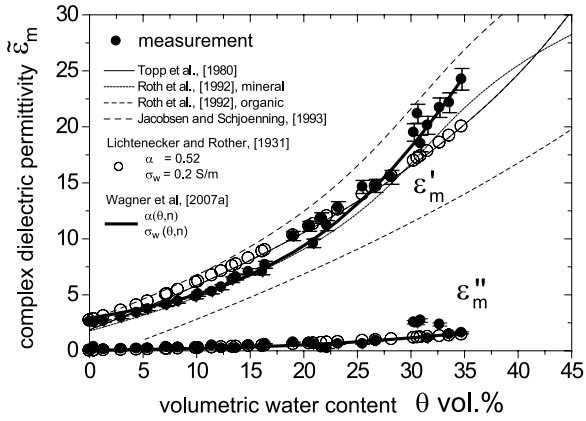

Figure 11. Complex relative effective dielectric permittivity $\tilde{\varepsilon}_m = \varepsilon'_m - j\varepsilon''_m$ at a measurement frequency of 1 GHz as a function of volumetric water content (T = 22°C).

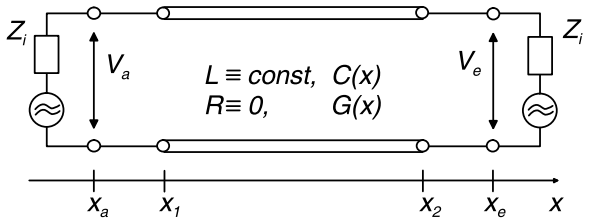

Figure 12. The nonuniform flat ribbon cable, situated between x_1 and x_2, is connected to two lossless uniform coaxial cables with matched impedances Z_i at their end points.

by material specific calibration functions (see Figure 11). The first step is a key component for the reconstruction procedure and will be discussed below in the procedure for two-ended TDR measurements. Detailed information about the reconstruction algorithm can be found in *Schlaeger* [2002, 2005].

2.4.2. Procedure for Two-Ended Measurements

[25] Figure 12 shows a schematic setup for receiving reflection data from both ends of the unknown material. The telegraph equation (4) describes the variation of voltage $V(x, t)$ and current $I(x, t)$ due to an incident voltage step along the transmission line. $C(x)$ and $G(x)$ are influenced by $\theta(x)$ along the waveguide. L is a function of the transmission line only and is assumed to be constant and known for coaxial and flat ribbon cable. Any resistance along the waveguide has been neglected. All parameters are given per unit of length.

$$\begin{aligned} \frac{\partial}{\partial x} V(x,t) &= -L \frac{\partial}{\partial t} I(x,t) \\ \frac{\partial}{\partial x} I(x,t) &= -G(x) V(x,t) - C(x) \frac{\partial}{\partial t} V(x,t) \end{aligned} \tag{4}$$

In order to reconstruct $C(x)$ and $G(x)$ simultaneously, two independent TDR measurements $V_1^{(m)}(x, t)$ and $V_2^{(m)}(x, t)$ are needed. To solve this inverse problem, the forward problem with full wave solution $V_1^{(s)}(x, t)$ and $V_2^{(s)}(x, t)$ is calculated for given distributions for $C(x)$ and $G(x)$. The simulated TDR reflectograms $V_i^{(s)}$ for both ends are compared between the first main reflection at $t = 0$ and the second main reflection at $t = T$ to the measurements $V_i^{(m)}$ using the objective function (5):

$$J(C,G) = \sum_{i=1}^{2} \int_0^T \left[V_i^{(s)}(x_i, t; C, G) - V_i^{(m)}(x_i, t) \right]^2 dt \tag{5}$$

The conjugate gradient method is used to minimize the objective function (5) with the inversion parameters $C(x)$ and $G(x)$. The gradient of this objective function can be calculated directly by means of the corresponding adjoint partial differential equation of equations (4) [*Schlaeger*, 2005]. The conjugate gradient is necessary to determine the improved distributions of $C(x)$ and $G(x)$, which are used for the next iteration step. This procedure is repeated until the objective function is minimized. The direct calculation of the gradients is one reason for the fast iterative search. However, during the optimization process it is necessary to calculate the solution of the forward problem for many different distributions of $C(x)$ and $G(x)$. Therefore it is also important to use an algorithm for the solution of partial differential equations that is computationally efficient to guarantee fast convergence. For example, the reconstruction of the water content distribution for a 2 m flat ribbon cable with a discretization of 2 mm requires approximately 90 min for 20 iteration steps on a 3.8 GHz computer and 2 GB RAM.

2.4.3. Reconstruction Example for an Artificial, Lossy Material

[26] The result of a numerical simulation is used for the verification of the reconstruction algorithm. In this way uncertainties, which are unavoidable during sampling in actual experiments, can be neglected. The transmission line with $C(x)$ and $G(x)$ is now considered as shown in Figure 13.

[27] The TDR reflections from the left and the right of the transmission line in Figure 13 are shown on the left of Figures 14a and 14b. For the opposite end of the transmission line an open circuit is used for each simulation, which results in a total reflection occurring at about 22 ns. In this example, the variation of the capacitance can be roughly estimated from the amplitude variations in the TDR trace. High amplitude means low capacitance and vice versa. Since two independent TDR traces are available, only measurements between first and second main reflections are necessary to reconstruct $C(x)$ and $G(x)$ [*He et al.*, 1994; *Rahman and Marklein*, 2005].

[28] As can be seen on the TDR traces, losses reduce signal energy and decrease the amplitude of the signal. The pronounced downward slope of the signal prevents an estimation of the capacitance profile by simple analysis of the amplitude variation. In a lossy case the reconstruction algorithm requires reflection data from both ends of the transmission line to achieve reasonable accuracy. The results shown on the right of Figure 14 approximate the true profiles for $C(x)$ and $G(x)$ to a satisfactory degree (see Figures 14c and 14d). Additional examples are given by *Schlaeger* [2005] and *Huebner et al.* [2005].

3. Examples of Measurements Taken on a Full-Scale Levee Model

3.1. Levee Model and Instrumentation

[29] The levee model is located at the Federal Waterways and Research Institute in Karlsruhe (see Figure 15a). It is constructed homogeneously with uniform sand (grain size 0.2–2 mm) with a pore volume of ~37% and is situated on a base consisting of a waterproof plastic sheet, so that water infiltrating into the levee body flows to a drain at the toe of the land-side slope (Figure 15c). The slope inclinations are 1:2.0 on the water side and 1:2.25 on the land side. Both slopes of the levee are covered with an approximately 20 cm thick topsoil layer. The discharge of the water collected in the drain is recorded in a monitoring and data collection container.

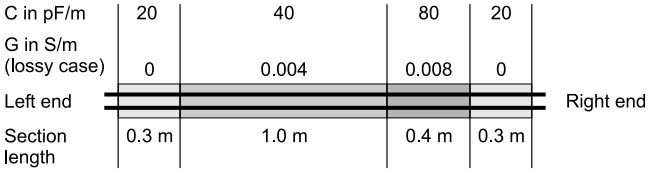

Figure 13. Sectionwise constant distribution of $C(x)$ and $G(x)$ for an artificial, lossy material.

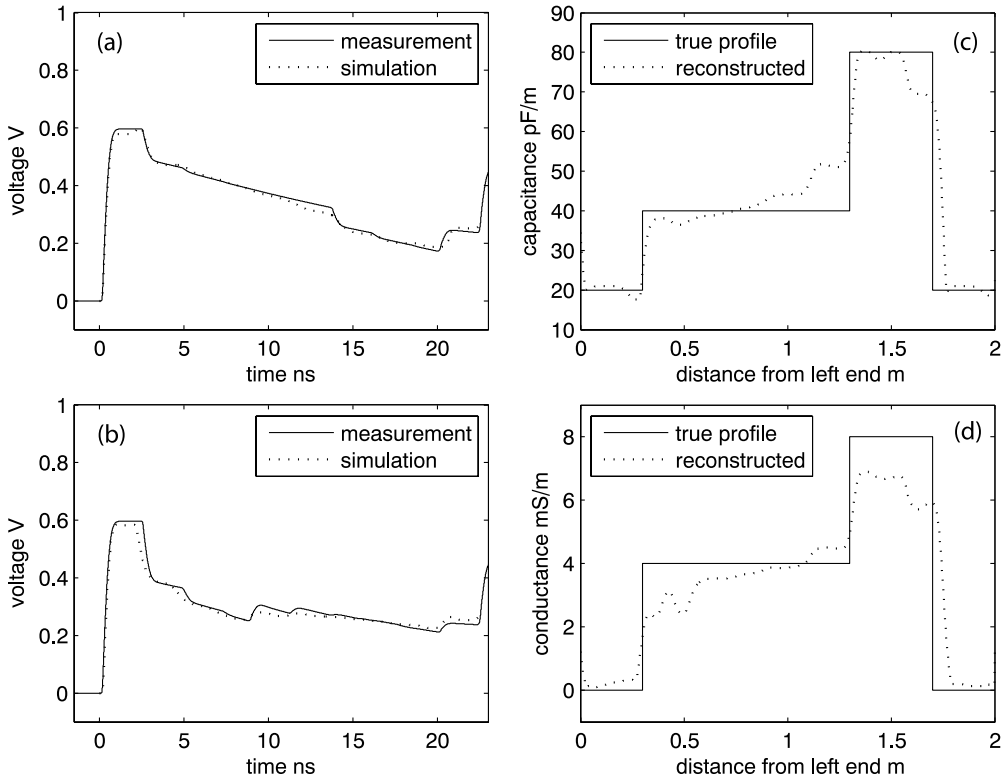

Figure 14. (left) TDR reflections measured from the (a) left and (b) right. (right) Reconstruction of (c) $C(x)$ and (d) $G(x)$ from two-ended data.

[30] In order to assess the pore water pressures within the levee body, the model is equipped with piezometer gauges which are also distributed along the base of the levee (Figure 15c). Twelve flat ribbon cables from 1 m to 3 m in length were installed vertically inside the levee body (Figure 15b). For this purpose, boreholes were sunk into the levee body down to the base and the cables were placed into the holes along one wall of the borehole. The coaxial cable, which was connected with the flat ribbon cable via an epoxy filled plastic box, was placed on the opposite side of the hole to prevent any disturbances to the sensitive area. The holes were filled up with more or less the same density as before using borrow material. This procedure was possible since the levee is constructed homogeneously with well-graded sand.

[31] Via a multiplexer the flat ribbon cables are connected with coaxial cables on both sides to a TDR device (Tektronix cable tester) located in a box on the crest of the levee. A conventional PC situated at the toe of the land-side slope automatically controls data collection and operation of the TDR device and multiplexer using a program created by the authors.

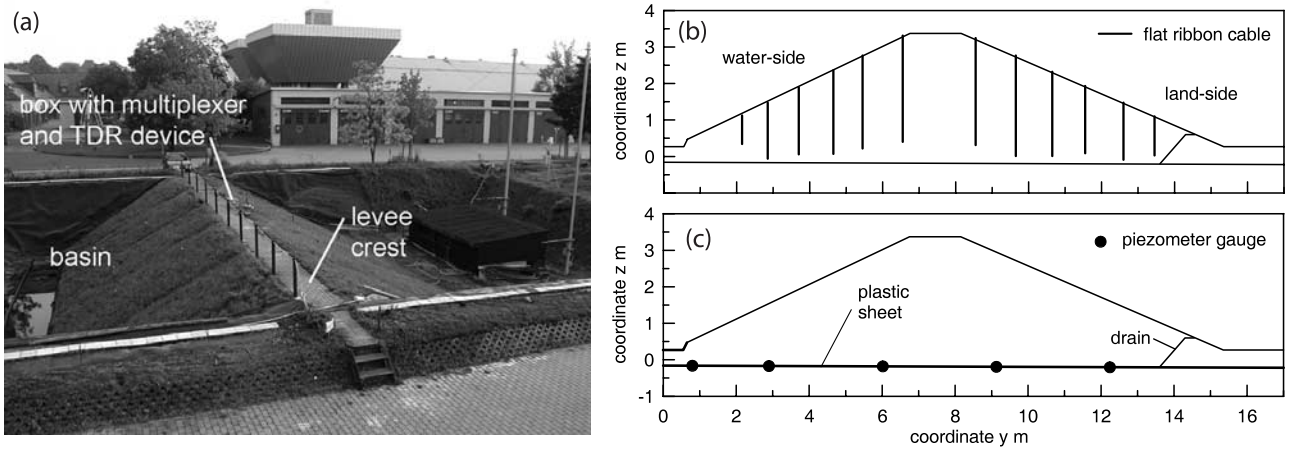

Figure 15. (a) Full-scale levee model (water side on the left) at the Federal Waterways and Research Institute in Karlsruhe, (b) positions and lengths of the flat ribbon cables in the cross section of the levee, and (c) positions of piezometer gauges.

With this system the data acquisition time for the whole cross section lasts only 5 min.

3.2. Measurement Examples

3.2.1. Overview

[32] Different experimental investigations were carried out on the levee model. Several flood simulation tests were conducted under different initial hydraulic conditions which were left unaltered or were artificially changed using sprinkler irrigation or by conducting a small precursory flood situation. Furthermore, long-term observations were made in order to investigate meteorologically influenced water balance processes. The access tube probe TRIME-T3 [*Laurent et al.*, 2005] from IMKO was used as the only comparison method for the spatial TDR system. With this probe it is possible to take manual water content measurements in plastic tubes. Six tubes are installed in one levee cross section near the cross section with the flat ribbon cables. The measurement results from flood simulation and sprinkler irrigation tests are presented in the following. The focus here lies on the spatial TDR measurements and the main findings from these results. Finally, two examples of water content measurements with different previous meteorological histories are presented.

3.2.2. Flood Simulation Test

[33] In December 2000 a flood simulation test was carried out with a natural water content distribution as the initial hydraulic condition. The transient evolution of the seepage water through the levee body can be observed by the water content distributions shown in Figures 16a–16c. The measured phreatic surface and the location of the transition of the water contents from the wet to the dry zone correspond very well. On the basis of this comparison an accuracy of the spatial resolution of ±3 cm can be derived. It is also possible to recognize the capillary border above the phreatic surface. The water contents measured during the stationary condition (Figures 16c and 16d) both with the flat ribbon cables and with the access tube probe from IMKO correspond well. In this regard, with both systems different values of water contents were recorded underneath the phreatic surface. The pore volume of the sand in the levee is about 37% which is equivalent to the volumetric water content at full saturation. The water contents below the phreatic surface measured with both systems are between 30 and 35% indicating a fairly high residual amount of air remaining in the pores. It is known that the amount of residual air in almost saturated conditions depends on the hydraulic conditions, which have led to the saturation, and can reach values of up to 20% of the pore volume [*Fredlund and Rahardjo*, 1993]. This qualitative empirical correlation verifies the observations made with these measurement systems.

3.2.3. Infiltration of Water Due to Precipitation

[34] An extreme precipitation event for Karlsruhe expected to occur once in every 100 years was simulated using sprinkler irrigation equipment. The irrigation was performed in three phases of 9 h each over a time period of 57 h. Figures 17a–17c show distributions of the volumetric water content during the irrigation test. The first phase started at midnight on 29 May 2002; the corresponding initial condition for the test is shown in Figure 17a. After 9 h of irrigation the measured water content distribution in Figure 17b showed a moisture front, which had infiltrated the levee body up to a depth of approximately 0.75 m. The irrigation phases were repeated at the same times during the following two nights.

[35] After the last irrigation phase (9:00 A.M. on 31 May 2002) the saturation distribution of Figure 17c was measured. It can be seen that despite the high quantity of irrigated water, no homogeneously distributed saturation was reached. In fact, the larger part of the water was stored near the surface in the slopes of the levee. Compared to the water content distribution of Figure 17c the water did not percolate much deeper into the levee body than a maximum depth of about 2 m. The consequence of the lateral water flow is an area in the middle of the cross section which remains nearly unchanged (Figure 17d). The explanation for this observation is that in the more saturated areas near the slope surface the sand has a higher hydraulic conductivity due to the higher water content, so that water can flow laterally to the waterproof sealing at the base of the levee, which is equivalent to a capillary barrier effect. Similar observations in comparatively homogeneous soils are reported by *McCord et al.* [1991]. The investigations on the levee model have also given indications of the occurrence of fingering during the sprinkler irrigation test [*Scheuermann*, 2005; *Scheuermann and Bieberstein*, 2007].

3.2.4. Long-Term Observations

[36] Since the beginning of 2000 water content changes have been observed continuously on the levee model. Apart from isolated sprinkler irrigation during the summer time to water the grass cover and a few flood simulation tests, the water content changes are mainly influenced by precipitation and evapotranspiration. Because of its construction it is possible to use the levee model as a lysimeter to investigate the meteorologically influenced water balance processes. Figure 18 shows examples of water content distribution in the levee model resulting from previous meteorological effects characterized by precipitation events. In addition the discharge through the levee is shown in the graphs. As can be seen, the water content distributions show distinctive differences not only concerning the mean volumetric water contents (given in the graphs), but also concerning the distribution of the water inside the levee body. In particular, it should be pointed out that after the precipitation period in March 2001 (see Figure 18 (left)) the water content primarily increased up to a certain depth as already shown for the precipitation experiment. The observations on the levee model have now already covered a time span of 7 years.

4. Discussion and Conclusion

[37] Spatial time domain reflectometry is a useful method for determining soil moisture profiles along buried transmission lines. A new sensor has been developed, which can be used in lengths up to several meters and which is less affected by the electrical conductivity of the surrounding soil than uncoated probes. The maximal length depends strongly on the surrounding material. In lossless sand a length of 5 m is realistic whereas lossy soil only allows a sensor length of about 3 m. A new reconstruction algorithm allows the calculation of moisture distributions from two-ended TDR measurements on the basis of transmission line models and soil specific calibrations.

[38] The use of spatial TDR in combination with flat ribbon cables as probes on the levee model has proven the feasibility of this method. It was possible to achieve a data

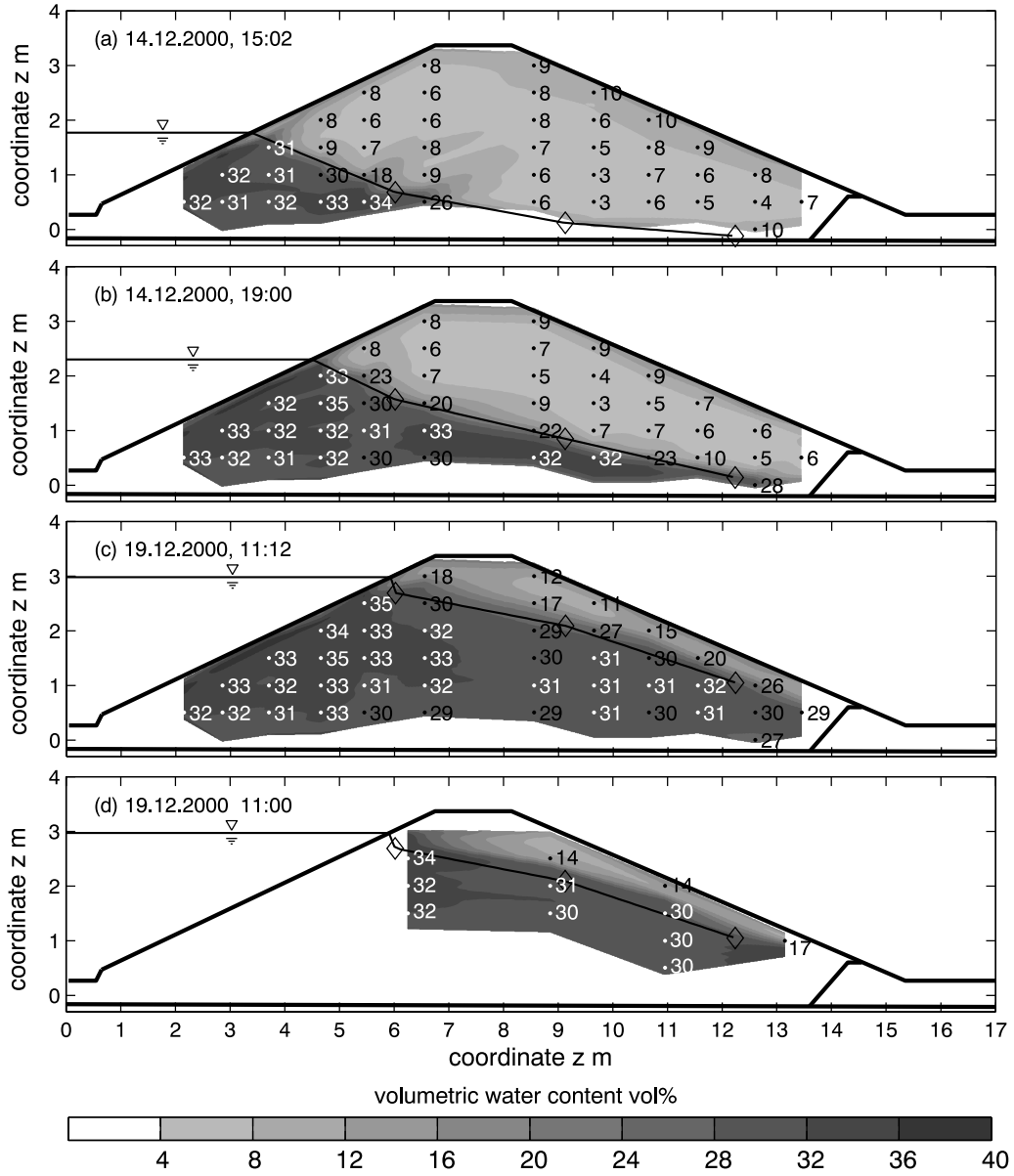

Figure 16. Measurements of the water content distribution inside the levee model during a flood simulation test: (a–c) transient development of the seepage measured with the flat ribbon cables and (d) water content distribution during the stationary seepage condition measured with the access tube probe from IMKO in comparison to Figure 16c. The vertical orientation of the dots represents the positions of the individual flat ribbon cables. The rhombuses show the hydraulic head measured by the pore water gauges in the base of the levee (Figure 15c) representing the approximate position of the phreatic line inside the levee body. The water level in the basin is measured independently.

acquisition time of about 5 min for measuring the complete cross section with the available measuring devices in the levee model. Because of this data acquisition, a quantitative monitoring of time transient water transport processes was achieved for the first time with this spatial resolution. The comparison of the results with the independent measurements of the phreatic surface measured with the pressure gauges at the base and the water contents recorded with the access tube probe have shown that (1) a spatial resolution of about 3 cm could be reached and (2) a quantification of the water contents was possible with an average deviation of about ±2 vol %.

[39] Although the quality of the results is very satisfactory, it should be pointed out here that they cannot be easily transferred to other materials or even other applications for the following reasons. (1) The subsequent instrumentation of the levee model with flat ribbon cables using simple boreholes was only possible, since the levee was constructed homogeneously with well-graded sand without any structures within the levee body. (2) The dielectric property of the sand shows no frequency-dependent behavior, which means that the influence of the length of the flat ribbon cables on the resulting permittivity is negligible. Thus it can be concluded, that the good quality of the measurements taken from the

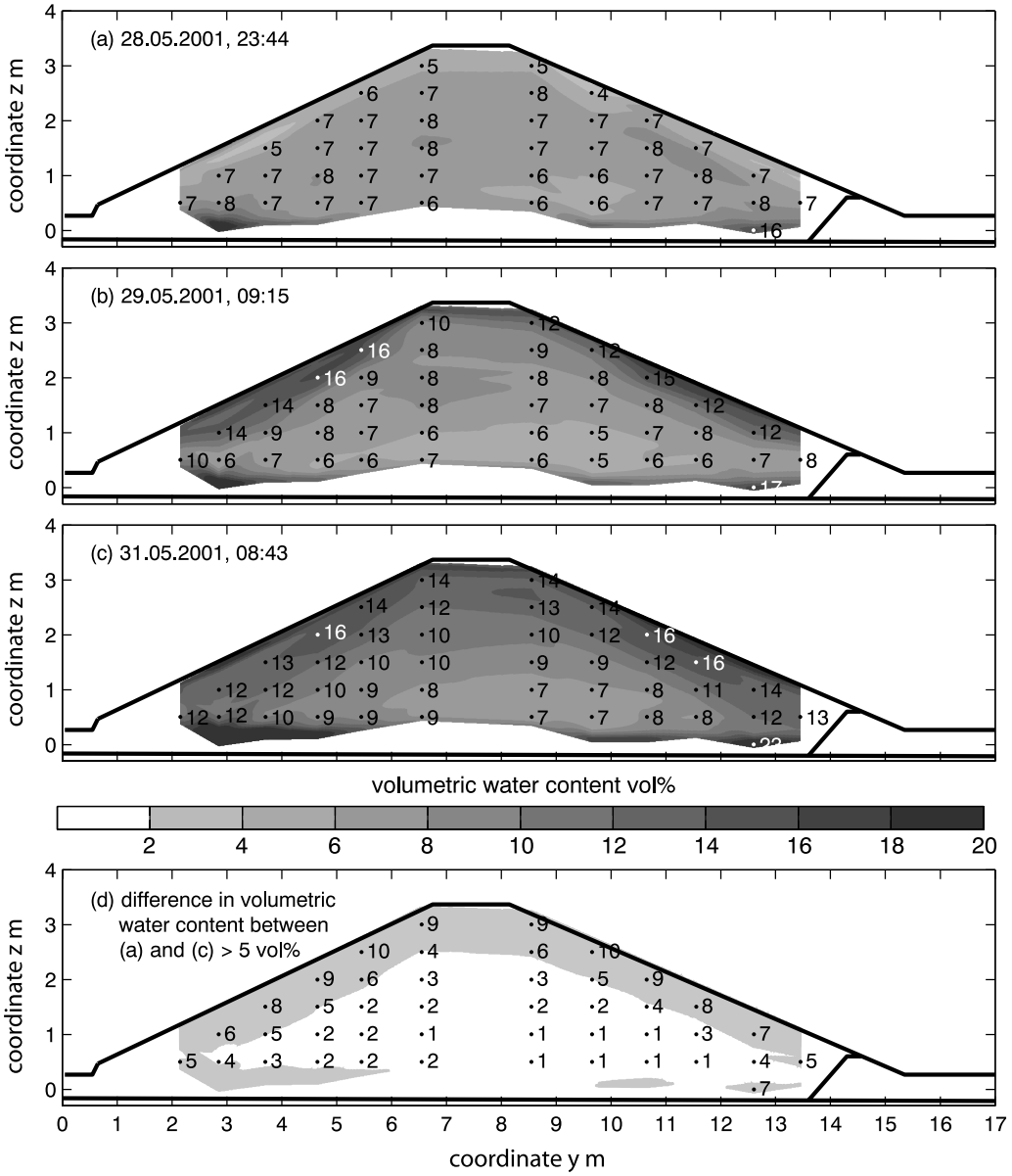

Figure 17. Distribution of saturation during an irrigation test (148 mm in 57 h) on the levee model (a) at the beginning of the irrigation test, (b) at the end of the first irrigation phase 9 h after the beginning of the experiment, and (c) at the end of the experiment and (d) the difference in the saturation between Figures 17a and 17c (area with changes >5% shaded).

levee model is based, to a certain extent, on the advantageous conditions mentioned.

[40] The spatial TDR method, consisting of the hardware TDR device and multiplexer, the calibration procedures for probes and for the soil and, as an essential part of the method, the reconstruction algorithm, has also been used in other applications especially for levees in the laboratory and in situ. In these applications, the necessity of improvements has become clear, and these are now partly under development or still remain to be carried out.

[41] 1. For the subsequent instrumentation of earth structures with flat ribbon cables, an installation method is necessary to permit soil to be preferably measured in an unchanged condition. For this purpose a method is under development using plastic tubes on which the flat ribbon cable is fixed. The tubes are placed in boreholes and filled with epoxy foam to press the sensor against the borehole [*Scheuermann et al.*, 2007]. The biggest problem at present is the prevention of a gap between sensor and soil. A similar method has been developed by *Dahan* [2005] for the measurement of mean water contents.

[42] 2. The three-dimensional numeric electromagnetic finite element simulation provides an informative basis for the sensor characteristics taking the frequency dependence of the measured complex dielectric permittivity into consideration [*Wagner et al.*, 2007a]. It has been shown that an air or water gap between sensor and soil already leads to dramatic under or overestimation of the water content with a mere gap thickness of 0.25 mm on both sides of the cable sensor. Therefore, the application of the flat ribbon cable as a

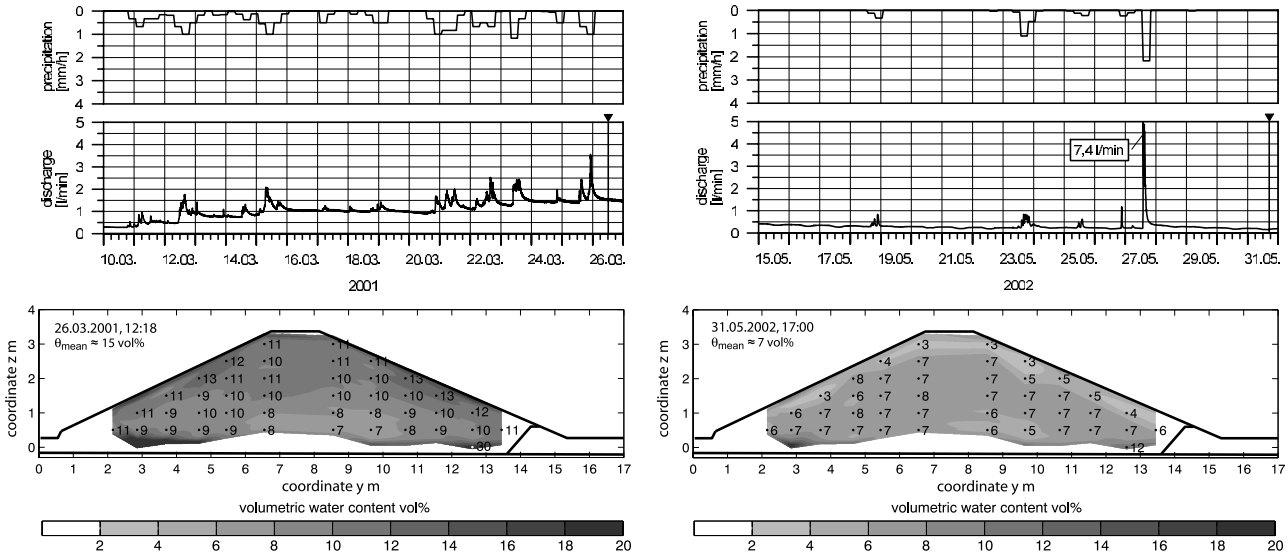

Figure 18. (bottom) Distributions of the volumetric water content inside the levee model with (top) meteorological effects over 16 days on (left) 26 March 2001 and (right) 31 May 2002.

moisture sensor requires an accurate installation technique of cable-like elements (especially for long sensors).

[43] 3. In order to take measurements in electrical lossy materials it is necessary to improve the probe to permit the localization of the ends of the probes, if a coaxial cable is connected at the distal end and dispersion is too high. The frequently used analysis method with tangents could fail under these conditions. For this purpose switches have been developed permitting a change in the electrical boundary at the ends of the probes. This technical advancement has led to an improved identification of the probe ends in the TDR trace using simple signal analysis methods [*Scheuermann et al.*, 2005]. Comparative investigations need to be performed to validate the resulting travel times.

[44] 4. Though the reconstruction algorithm considers conductivity in inverse modeling, dispersion has still been neglected so far. This should be included in future improvements.

[45] 5. The frequency-dependent relaxation behavior of soils should be used on the basis of sophisticated calibration procedures for the soil properties, in order to investigate the influence of the probe lengths on the quantification of the resulting water contents.

[46] The technical devices necessary for achieving TDR measurements, especially for monitoring purposes in the field, need to be improved. This includes the TDR device, which is still too expensive to allow large-scale applications, the multiplexers, which also have to work under extreme conditions (temperature, humidity), as well as controlling and data collection (PC suitable for field applications) and the current supply.

[47] Although open questions remain and improvements are still necessary, the examples given have proven the capability of the method. The future aim is to broaden the application area of the method which goes along with the improvements of the method outlined before. As the constellation of the group of authors shows, this is a task which requires an interdisciplinary approach.

[48] **Acknowledgments.** We greatly appreciate the opportunity of being able to perform the presented investigations on the levee model at the Federal Waterways and Research Institute (Bundesanstalt für Wasserbau) in Karlsruhe. Here we would especially like to express our gratitude to Heinrich Armbruster-Veneti, Michael Heibaum, and Bernhard Odenwald.

References

Abbaspour, K., R. Kasteel, and R. Schuh (2000), Inverse parameter estimation in a layered unsaturated field soil, *Soil Sci.*, *165*, 109–123, doi:10.1097/00010694-200002000-00002.

Asano, M., S. Sudo, N. Shinyashiki, S. Yagihara, T. Ohe, N. Morimoto, and K. Fujita (2007), Studies of dielectric properties of bentonite obtained by broadband dielectric spectroscopy, in *Seventh International Conference on Electromagnetic Wave Interaction with Water and Moist Substances*, edited by S. Okamura et al., pp. 25–30, Shizuoka Univ., Hamamatsu, Japan.

Becker, R. (2004), Spatial time domain reflectometry for monitoring transient moisture profiles, Ph.D. thesis, 257 pp., Inst. for Water and River Basin Manage., Univ. of Karlsruhe, Karlsruhe, Germany.

Behari, J. (2005), *Microwave Dielectric Behavior of Wet Soils*, *Remote Sens. Digital Image Process.*, vol. 8, Springer, New York.

Boyarskii, D., V. Tikhonov, and N. Komarova (2002), Model of dielectric constant of bound water in soil for applications of microwave remote sensing, *J. Electromagn. Waves Appl.*, *16*, 411–412, doi:10.1163/156939302X01227.

Buchner, R., J. Barthel, and J. Stauber (1999), The dielectric relaxation of water between 0°C and 35°C, *Chem. Phys. Lett.*, *306*, 57–63, doi:10.1016/S0009-2614(99)00455-8.

Dahan, O. (2005), Flexible probe for measuring moisture content in soils, Patent US 6956381 B2, U.S. Patent and Trademark Off., Washington, D. C.

Dalton, F. N., and M. T. van Genuchten (1986), The time-domain reflectometry method for measuring soil water content and salinity, *Geoderma*, *38*, 237–250, doi:10.1016/0016-7061(86)90018-2.

Davis, J., and A. Annan (1977), Electromagnetic detection of soil moisture—Progress report I, *Can. J. Remote Sens.*, *3*, 76–86.

Evett, S. R., and G. W. Parkin (2005), Advances in soil water content sensing: The continuing maturation of technology and theory, *Vadose Zone J.*, *4*, 986–991, doi:10.2136/vzj2005.0099.

Feng, W., C. P. Lin, R. J. Deschamps, and V. P. Drnevich (1999), Theoretical model of a multisection time domain reflectometry measurement system, *Water Resour. Res.*, *35*, 2321–2332, doi:10.1029/1999WR900123.

Ferré, P. A., H. H. Nissen, and J. Simunek (2002), The effect of the spatial sensitivity of TDR on inferring soil hydraulic properties from water content measurements made during the advance of a wetting front, *Vadose Zone J.*, *1*, 281–288.

Fredlund, D. G., and H. Rahardjo (1993), *Soil Mechanics for Unsaturated Soils*, John Wiley, New York.

Friedman, S. (1998), A saturation degree-dependent composite spheres model for describing the effective dielectric constant of unsaturated porous media, *Water Resour. Res.*, *34*, 2949–2961, doi:10.1029/98WR01923.

Greco, R. (2006), Soil water content inverse profiling from single TDR waveforms, *J. Hydrol.*, *317*, 325–339, doi:10.1016/j.jhydrol.2005.05.024.

Gutina, A., T. Antropova, E. Rysiakiewicz-Pasek, K. Virnik, and Y. Feldman (2003), Dielectric relaxation in porous glasses, *Microporous Mesoporous Mater.*, *58*, 237–254, doi:10.1016/S1387-1811(02)00651-0.

Hakansson, G. (1997), Reconstruction of soil moisture profiles, M.S. thesis, Dep. of Electromagn. Theory, R. Inst. of Technol., Stockholm.

He, S., V. G. Romanov, and S. Stroem (1994), Analysis of the Green's function approach to one-dimensional inverse problems. II. Simultaneous reconstruction of two parameters, *J. Math. Phys. N. Y.*, *35*, 2315–2335, doi:10.1063/1.530555.

Heimovaara, T. J., and W. Bouten (1990), A computer-controlled 36-channel time domain reflectometry system for monitoring soil water contents, *Water Resour. Res.*, *26*, 2311–2316.

Heimovaara, T. J., J. A. Huisman, J. A. Vrugt, and W. Bouten (2004), Obtaining the spatial distribution of water content along a TDR probe using the SCEM-UA Bayesian inverse modeling scheme, *Vadose Zone J.*, *3*, 1128–1145.

Hilhorst, M., C. Dirksen, F. Kampers, and R. Feddes (2001), Dielectric relaxation of bound water versus soil matric pressure, *Soil Sci. Soc. Am. J.*, *65*, 311–314.

Hoekstra, P., and A. Delaney (1974), Dielectric properties of soils at UHF and microwave frequencies, *J. Geophys. Res.*, *79*, 1699–1708, doi:10.1029/JB079i011p01699.

Hook, W. R., N. J. Livingston, Z. J. Sun, and P. B. Hook (1992), Remote diode shorting improves measurement of soil water by time domain reflectometry, *Soil Sci. Soc. Am. J.*, *56*, 1384–1391.

Huebner, C. (1999), Entwicklung hochfrequenter Messverfahren zur Bodenfeuchtebestimmung, *Sci. Rep. FZKA 6329*, pp., Forschungszent. Karlsruhe, Karlsruhe, Germany.

Huebner, C., and A. Brandelik (2000a), Distinguished problems in soil and snow aquametry, in *Sensors Update*, edited by H. Baltes, W. Göpel, and J. Hesse, pp. 317–340, John Wiley, Weinheim, Germany.

Huebner, C., and A. Brandelik (2000b), Near surface moisture sensing, in *Surface Sensing Technologies and Applications*, edited by C. Nguyen, *Proc. SPIE*, *4129*, 88–96.

Huebner, C., and K. Kupfer (2007), Modelling of electromagnetic wave propagation along transmission lines in inhomogeneous media, *Meas. Sci. Technol.*, *18*, 1147–1154, doi:10.1088/0957-0233/18/4/023.

Huebner, C., S. Schlaeger, R. Becker, A. Scheuermann, A. Brandelik, W. Schaedel, and R. Schuhmann (2005), Advanced measurement methods in time domain reflectometry for soil moisture determination, in *Electromagnetic Aquametry*, edited by K. Kupfer, pp. 317–347, Springer, Berlin.

Huisman, J. A., J. J. J. C. Snepvangers, W. Bouten, and G. B. M. Heuvelink (2003), Monitoring temporal development of spatial soil water content variation: Comparison of ground penetrating radar and time domain reflectometry, *Vadose Zone J.*, *2*, 519–529.

Ishida, T., T. Makino, and C. Wang (2000), Dielectric-relaxation spectroscopy of kaolinite, montmorillonite, allophane and imogolite under moist conditions, *Clays Clay Miner.*, *48*, 75–84, doi:10.1346/CCMN.2000.0480110.

Ishida, T., M. Kawase, K. Yagi, J. Yamakawa, and K. Fukada (2003), Effects of the counterion on dielectric spectroscopy of a montmorillonite suspension over the frequency range 10^5–10^{10} Hz, *J. Colloid Interface Sci.*, *268*, 121–126, doi:10.1016/S0021-9797(03)00688-X.

Jacobsen, O. H., and P. Schjønning (1993), Field evaluation of time domain reflectometry for soil water measurement, *J. Hydrol.*, *151*, 159–172, doi:10.1016/0022-1694(93)90234-Z.

Kaatze, U. (2005), Electromagnetic wave interactions with water and aqueous solutions, in *Electromagnetic Aquametry*, edited by K. Kupfer, pp. 15–37, Springer, Berlin.

Katsube, T. J., and L. S. Collet (1974), Electromagnetic propagation characteristics of rocks, in *The Physics and Chemistry of Minerals and Rocks*, edited by R. G. J. Strens, pp. 279–295, John Wiley, London.

Kirsch, R. (Ed.) (2006), *Groundwater Geophysics*, Springer, Berlin.

Lambot, S., M. Antoine, I. van den Bosch, E. C. Slob, and M. Vanclooster (2004), Electromagnetic inversion of GPR signals and subsequent hydrodynamic inversion to estimate effective vadose zone hydraulic properties, *Vadose Zone J.*, *3*, 1072–1081.

Laurent, J.-P. (2000), Profiling water content in soils by TDR: Experimental comparison with the neutron probe technique, *IAEA-TECDOC-1137*, Int. At. Energy Agency, Vienna.

Laurent, J.-P., P. Ruelle, L. Delage, A. Zaïri, B. Ben Nouna, and T. Adjmi (2005), Monitoring soil water content profiles with a commercial TDR system: Comparative field tests and laboratory calibration, *Vadose Zone J.*, *4*, 1030–1036, doi:10.2136/vzj2004.0144.

Leidenberger, P., B. Oswald, and K. Roth (2006), Efficient reconstruction of dispersive dielectric profiles using time domain reflectometry (TDR), *Hydrol. Earth Syst. Sci.*, *10*, 209–232.

Li, A. G., Z. Q. Yue, L. G. Tham, C. F. Lee, and K. T. Law (2005), Field-monitored variations of soil moisture and matric suction in a saprolite slope, *Can. Geotech. J.*, *42*, 13–26, doi:10.1139/t04-069.

Lichtenecker, K., and K. Rother (1931), Die Herleitung des logarithmischen Mischungsgesetzes aus allgemeinen Prinzipien der stationaeren Stroemung, *Phys. Z.*, *32*, 255–260.

Logsdon, S. D. (2005), Soil dielectric spectra from vector network analyzer data, *Soil Sci. Soc. Am. J.*, *69*, 983–989.

Long, D. S., J. M. Wraith, and G. Kegel (2002), A heavy-duty time domain reflectometry soil moisture probe for use in intensive field sampling, *Soil Sci. Soc. Am. J.*, *66*, 396–401.

Lundstedt, J., and S. He (1996), A time-domain optimization technique for the simultaneous reconstruction of the characteristic impedance, resistance and conductance of a transmission line, *J. Electromagn. Waves Appl.*, *10*, 581–602, doi:10.1163/156939396X01143.

Lundstedt, J., and M. Norgren (2003), Comparison between frequency domain and time domain methods for parameter reconstruction on nonuniform dispersive transmission lines, *Prog. Electromagn. Res.*, *43*, 1–37, doi:10.2528/PIER03020301.

Lundstedt, J., and S. Stroem (1996), Simultaneous reconstruction of two parameters from the transient response of a nonuniform LCRG transmission line, *J. Electromagn. Waves Appl.*, *10*, 19–50, doi:10.1163/156939396X00199.

McCord, J. T., D. B. Stephens, and J. L. Wilson (1991), Hysteresis and state-dependent anisotropy in modeling unsaturated hillslope hydrologic processes, *Water Resour. Res.*, *27*, 1501–1518, doi:10.1029/91WR00880.

Norgren, M., and S. He (1996), An optimization approach to the frequency-domain inverse problem for a nonuniform LCRG transmission line, *IEEE Trans. Microwave Theory Tech.*, *44*, 1503–1507, doi:10.1109/22.536038.

Nyfors, E., and P. Vainikainen (1989), *Industrial Microwave Sensors*, Artech House, Norwood, Mass.

Oswald, B. (2000), Full wave solution of inverse electromagnetic problems, Ph.D. thesis, Swiss Fed. Inst. of Technol, Zurich, Switzerland.

Rahman, M., and R. Marklein (2005), Time-domain techniques for computation and reconstruction of one-dimensional profiles, *Adv. Radio Sci.*, *3*, 219–225.

Regalado, C. (2006), A geometrical model of bound water permittivity based on weighted averages: The allophane analogue, *J. Hydrol.*, *316*, 98–107, doi:10.1016/j.jhydrol.2005.04.014.

Robinson, D. A., S. B. Jones, J. M. Wraith, D. Or, and S. P. Friedman (2003), A review of advances in dielectric and electrical conductivity measurement in soils using time domain reflectometry, *Vadose Zone J.*, *2*, 444–475.

Roth, C. H., M. A. Malicki, and R. Plagge (1992), Empirical evaluation of the relationship between soil dielectric constant and volumetric water content as the basis for calibrating soil moisture measurements by TDR, *J. Soil Sci.*, *43*, 1–13, doi:10.1111/j.1365-2389.1992.tb00115.x.

Roth, K., R. Schulin, H. Fluehler, and W. Attinger (1990), Calibration of time domain reflectometry for water content measurement using a composite dielectric approach, *Water Resour. Res.*, *26*, 2267–2273.

Rothe, A., W. Weis, K. Kreutzer, D. Matthies, U. Hess, and B. Ansorge (1997), Changes in soil structure caused by the installation of time domain reflectometry probes and their influence on the measurement of soil moisture, *Water Resour. Res.*, *33*, 1585–1593, doi:10.1029/97WR00677.

Schaedel, W. (2006), Schritte zur Verbesserung der Hochwasserfruehwarnung mittels Online-Bodenfeuchtemessungen, Ph.D. thesis, 186 pp., Inst. for Water and River Basin Manage., Univ. of Karlsruhe, Karlsruhe, Germany.

Scheuermann, A. (2005), Instationaere Durchfeuchtung quasi-homogener Erddeiche, Ph.D. thesis, 290 pp., Inst. for Soil Mech. and Rock Mech., Univ. of Karlsruhe, Karlsruhe, Germany.

Scheuermann, A. (2008), Water content dynamics in unsaturated soils—Results of experimental investigations in laboratory and in situ, in *Unsaturated Soils: Advances in Geo-Engineering*, edited by D.G. Toll, pp. 197–204, Francis and Taylor, London.

Scheuermann, A., and A. Bieberstein (2006), Monitoring of dams and dikes—Water content determination using time domain reflectometry (TDR), in *13th Danube-European Conference on Geotechnical Engineering*, edited by J. Logar et al., pp. 493–498, Slovenian Geotech. Soc., Ljubljana, Slovenia.

Scheuermann, A., and A. Bieberstein (2007), Preferential water movement in homogeneous soils, in *Experimental Unsaturated Soil Mechanics*, *Springer Proc. Phys.*, vol. 112, edited by T. Schanz, pp. 461–473, Springer, Berlin.

Scheuermann, A., and C. Huebner (2009), On the feasibility of pressure profile measurement, *IEEE Trans. Instrum. Meas.*, *58*(2), 467–474.

Scheuermann, A., S. Schlaeger, C. Huebner, A. Brandelik, and J. Brauns (2001), Monitoring of the spatial soil water distribution on a full-scale dike model, in *Fourth International Conference on Electromagnetic Wave Interaction with Water and Moist Substances*, edited by K. Kupfer and C. Huebner, pp. 343–350, Mater. Res. and Testing Inst., Bauhaus Univ. Weimar, Weimar, Germany.

Scheuermann, A., S. Schlaeger, R. Becker, and A. Bieberstein (2005), Measurement of moisture content in a highly electrical lossy material using time domain reflectometry, in *Sixth International Conference on Electromagnetic Wave Interaction With Water and Moist Substances*, edited by K. Kupfer et al., pp. 166–173, Mater. Res. and Testing Inst., Bauhaus Univ. Weimar, Weimar, Germany.

Scheuermann, A., A. Bieberstein, C. Huebner, R. Becker, and S. Schlaeger (2007), Monitoring von Altdeichstrecken—Instrumentierung eines 250 m langen Deichabschnittes mit TDR-Sensoren zur Bestimmung von Feuchteverteilungen, in *Innovative Feuchtemessung in Forschung und Praxis 3*, edited by F. Nestmann, pp. 83–89, Aedificatio, Freiburg, Germany.

Scheuermann, A., A. Bieberstein, T. Triantafyllidis, C. Huebner, R. Becker, S. Schlaeger, and N. Wagner (2008), Spatial time domain reflectometry (spatial TDR)—On the use in geotechnics and geohydraulics, in *Unsaturated Soils: Advances in Geo-Engineering*, edited by D. G. Toll, pp. 189–196, Francis and Taylor, London.

Schlaeger, S. (2002), Inversion von TDR-Messungen zur Rekonstruktion raeumlich verteilter bodenphysikalischer Parameter, Ph.D. thesis, 189 pp., Inst. for Soil Mech. and Rock Mech., Univ. of Karlsruhe, Karlsruhe, Germany.

Schlaeger, S. (2005), A fast TDR-inversion technique for the reconstruction of spatial soil moisture content, *Hydrol. Earth Syst. Sci.*, *9*, 481–492.

Schofield, T. G. (2001), Long-term stability of time domain reflectometry measurements in a multi-year field experiment, paper presented at Second International Symposium and Workshop on Time Domain Reflectometry for Innovative Geotechnical Applications, Northwestern Univ., Evanston, Ill., 5–7 Sept.

Serbin, G., and D. Or (2003), Near-surface soil water content measurements using horn antenna radar: Methodology and overview, *Vadose Zone J.*, *2*, 500–510.

Shen, L., H. Marouni, Y. Zhang, and X. Shi (1987), Analysis of the parallel-disk sample holder for dielectric permittivity measurement, *IEEE Trans. Geosci. Remote Sens.*, *25*, 534–540, doi:10.1109/TGRS.1987.289831.

Sihvola, A. (2000), *Electromagnetic Mixing Formulae and Applications*, *IEE Electromagn. Waves Ser.*, vol. 47, Inst. of Eng. and Technol., Stevenage, U.K.

Stacheder, M. (1996), Die Time Domain Reflectometry in der Geotechnik—Messungen von Wassergehalt, elektrischer Leitfaehigkeit und Strofftransport, Ph.D. thesis, 170 pp., Inst. for Appl. Geol., Univ. of Karlsruhe, Karlsruhe, Germany.

Stacheder, M., C. Huebner, S. Schlaeger, and A. Brandelik (2005), Combined TDR and low frequency permittivity measurements for continuous snow wetness and snow density determination, in *Electromagnetic Aquametry*, edited by K. Kupfer, pp. 367–382, Springer, Berlin.

Stenger, R., T. Woehling, G. Barkle, and A. Wall (2007), Relationship between dielectric permittivity and water content for vadose zone materials of volcanic origin, *Aust. J. Soil Res.*, *45*, 299–309, doi:10.1071/SR06172.

Todoroff, P., and J.-D. Lan Sun Luk (2001), Calculation of in situ soil water content profiles from TDR signal traces, *Meas. Sci. Technol.*, *12*, 27–36, doi:10.1088/0957-0233/12/1/304.

Topp, G. C., J. L. Davis, and A. Annan (1980), Electromagnetic determination of soil water content: Measurement in coaxial transmission lines, *Water Resour. Res.*, *16*, 574–582, doi:10.1029/WR016i003p00574.

Topp, G. G., J. L. Davis, and A. P. Annan (1982), Electromagnetic determination of soil water content using TDR: I. Applications to wetting fronts and steep gradients, *Soil Sci. Soc. Am. J.*, *46*, 672–678.

Vereecken, H., R. Kasteel, J. Vanderborght, and T. Harter (2007), Upscaling hydraulic properties and soil water flow processes in heterogeneous soils: A review, *Vadose Zone J.*, *6*, 1–28, doi:10.2136/vzj2006.0055.

Wagner, N., E. Trinks, and K. Kupfer (2007a), Determination of the spatial TDR-sensor characteristics in strong dispersive subsoil using 3D-FEM frequency domain simulations in combination with microwave dielectric spectroscopy, *Meas. Sci. Technol.*, *18*, 1137–1146, doi:10.1088/0957-0233/18/4/022.

Wagner, N., K. Kupfer, and E. Trinks (2007b), A broadband dielectric spectroscopy study of the relaxation behaviour of subsoil, in *Seventh International Conference on Electromagnetic Wave Interaction with Water and Moist Substances*, edited by S. Okamura et al., pp. 31–38, Shizuoka Univ., Hamamatsu, Japan.

Wagner, N., K. Kupfer, and E. Trinks (2007c), Electromagnetic material properties of moist soil determined by broadband dielectric spectroscopy, in *Innovative Feuchtemessung in Forschung und Praxis 3*, edited by F. Nestmann, pp. 37–45, Aedificatio, Freiburg, Germany.

Wang, J., and T. Schmugge (1980), An empirical model for the complex dielectric permittivity of soils as a function of water content, *IEEE Trans. Geosci. Remote Sens.*, *18*, 288–295, doi:10.1109/TGRS.1980.350304.

Whalley, W. R. (1993), Considerations on the use of time-domain reflectometry (TDR) for measuring soil water content, *Eur. J. Soil Sci.*, *44*, 1–9, doi:10.1111/j.1365-2389.1993.tb00429.x.

Woersching, H., R. Becker, S. Schlaeger, A. Bieberstein, and P. Kudella (2006), Spatial TDR moisture measurement in a large scale levee model made of loamy soil material, paper presented at TDR 2006, Purdue Univ., West Lafayette, Indiana. (Available at https://engineering.purdue.edu/TDR/Papers)

R. Becker, IMKO GmbH, Im Stöck 2, Ettlingen D-76275, Germany.

A. Bieberstein and A. Scheuermann, Institute for Soil Mechanics and Rock Mechanics, Karlsruhe Institute of Technology, Universität Karlsruhe, Engler-Bunte-Ring 14, D-76131 Karlsruhe, Germany. (alexander.scheuermann@ibf.uka.de)

C. Huebner, Institute for Industrial Data Processing and Communication, University of Applied Sciences, Paul-Wittsack-Strasse 10, D-68163 Mannheim, Germany.

S. Schlaeger, Mathematical Solutions and Engineering, Lammbergweg 23, Horn-Bad Meinberg, D-32805, Germany.

N. Wagner, Institute of Material Research and Testing, Bauhaus-University Weimar, Coudraystrasse 6, D-99423 Weimar, Germany.